Remarkable Thermal Stability of Gold Nanoparticles Functionalised with Ruthenium Phthalocyanine Complexes

Shirin R. King, Susan Shimmon, Angus R. Gentle, Mika T. Westerhausen, Annette Dowd, Andrew M. McDonagh*

School of Mathematical and Physical Sciences, University of Technology Sydney, Broadway,
Ultimo, NSW 2007 Australia

Corresponding author email address: andrew.mcdonagh@uts.edu.au

Abstract

A gold nanoparticle (AuNP) ruthenium phthalocyanine (RuPc) nanocomposite has been synthesised that exhibits high thermal stability. Electrical resistance measurements revealed that the nanocomposite is stable up to ~320 °C. Examination of the nanocomposite and the RuPc stabiliser complex using thermogravimetric analysis and differential scanning calorimetry show that the remarkable thermal stability is due to the RuPc molecules, which provide an effective barrier to sintering of the AuNPs.

Keywords: Gold nanoparticles, sintering, ruthenium phthalocyanine

Introduction

Gold nanoparticles (AuNPs) functionalised with a wide range of molecules have attracted significant interest in recent decades due to their useful and tunable optical properties, ease of synthesis, and diverse applications [1–4]. The sintering of gold nanoparticles has been examined in detail due to applications in the fabrication of electrically conducting structures at moderate to low temperatures [5–7]. In such applications, particles must remain separated until a stimulus is applied (often heat or light) to initiate sintering, whereupon quite conductive gold structures can be produced [8–10]. Various "lightly-stabilised" particles for this application are now commercially available. In contrast, relatively little is known about gold nanoparticles with a much higher degree of thermal stability. Particles that are resistant to sintering are important in applications where it is desirable for useful properties (e.g., optical or catalytic) to be retained at higher temperatures. One strategy to achieve such resistance is to coat the gold particles in an inorganic oxide shell [11–14]. Inorganic coatings are quite thermally robust but may induce changes in optical properties and/or affect subsequent surface functionalisation.

Recently, the effects of functionalising AuNPs with phthalocyanine (Pc) molecules have been explored [15,16]. Pc complexes are a class of dye with very strong optical absorption bands and have applications as organic conductors, catalysts and as photosensitisers in photodynamic therapy [17]. In addition, Pcs can have high thermal stabilities [18], making them promising candidates for stabilisers of AuNPs that may resist sintering at high temperatures.

Here we present our investigations into gold nanoparticles functionalised with ruthenium phthalocyanine complexes. The resultant nanocomposites maintain the intense optical absorbance characteristics of the RuPc complex and also prove to be resistant to sintering at

temperatures up to 320 °C. Not only does this nanocomposite provide a new capability in environments where heating (localised or general) to reasonably high temperatures may occur, it also offers a functional coating that switches from insulating to conductive at a critical temperature threshold far above that of currently available gold sinter ink materials.

Results and Discussion

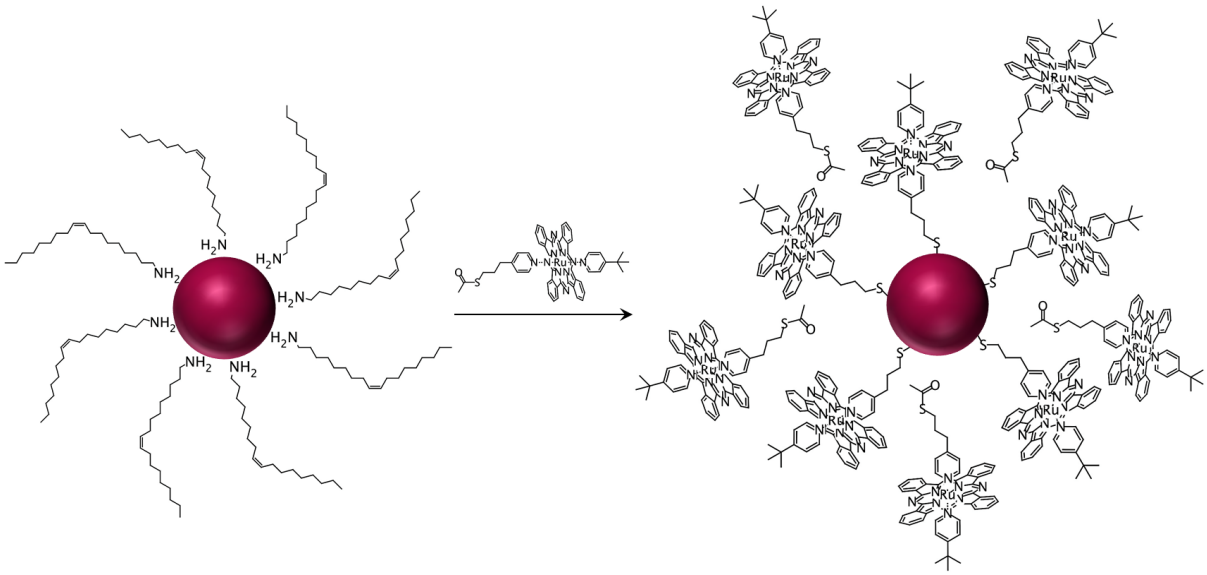

Scheme 1. Synthesis of the RuPc-AuNP nanocomposite.

A gold nanoparticle/RuPc nanocomposite was prepared by the addition of the new complex [RuPc(4-py$(CH_2)_3$SAc)(4-py^{t}Bu)] (Scheme 1) to oleylamine-stabilised gold nanoparticles. The ruthenium phthalocyanine complex bears thioacetate groups capable of binding to gold surfaces [19] via cleavage of the acetate groups and thus displaces the more weakly-bound amine stabiliser molecules as illustrated in Scheme 1. The complex also bears a 4-*tert*-butylpyridine ligand to enhance solubility in organic solvents. The resultant particles were quite stable when subjected to centrifugation/resuspension cycles using ethanol. This process could be repeated at least ten times after which the particles could still be readily resuspended.

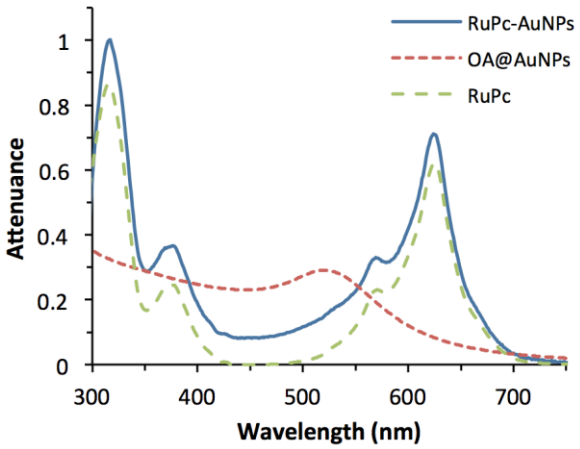

Figure 1. UV-visible absorption spectra of RuPc-AuNPs compared to both oleylamine-stabilised AuNPs and [RuPc(4-py$(CH_2)_3$SAc)(4-py^{t}Bu)] (arbitrary scaling).

The RuPc-AuNPs could be resuspended in solvents such as toluene or dichloromethane and the suspensions were intense blue in colour, in contrast to the red colour of the oleylamine-stabilised particles. The blue colour arises from the intense optical absorption of the RuPc complex at 625 nm rather than from aggregation of the particles (which can cause a bathochromic shift of the plasmon resonance wavelength) [20]. The UV-visible spectrum of the RuPc-AuNPs is shown in Figure 1. The spectrum displays similar features to that of the unbound RuPc complex (Figure 1), with an additional absorbance band at 520 nm, which is assigned to the AuNPs. The RuPc spectrum is consistent with the spectra reported for ruthenium phthalocyanine complexes [17]. A strong Q-band absorption is observed at 625 nm, and an intense Soret band (B-band) is found at 316 nm, both of which have been assigned to $\pi \rightarrow \pi^*$ transitions within the Pc macrocycle. Both bands are accompanied by weaker peaks at 570 nm and 377 nm, respectively. These absorption bands have been ascribed to charge transfer transitions, though their exact nature is uncertain [21].

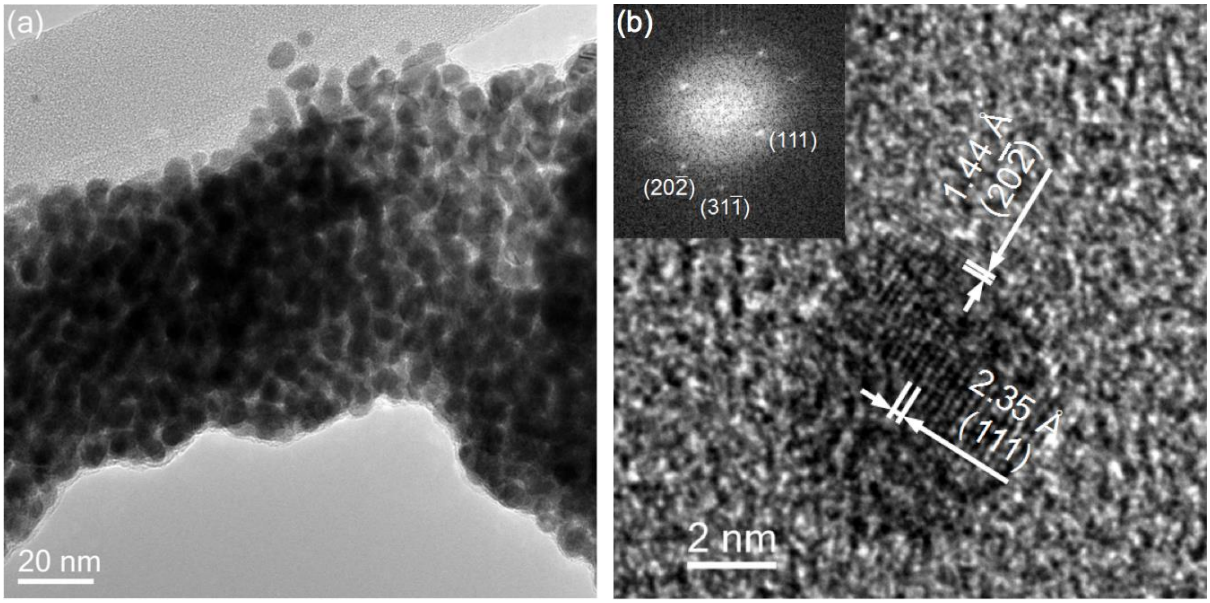

Figure 2. Transmission electron micrographs of (a) nanocomposite containing 5 nm diameter gold particles functionalised with [RuPc(4-py$(CH_2)_3$SAc)(4-py^{t}Bu)] and (b) a twinned fcc gold nanoparticle oriented close to [1$\bar{2}$1]. The inset shows the FFT.

The RuPc-AuNPs were characterised with transmission electron microscopy (TEM). Figure 2(a) shows a drop cast film containing functionalised gold nanoparticles. The average size was determined to be 5.3 nm with a standard deviation of 1.0 nm, which is similar in size to the oleylamine-stabilised particles. Energy dispersive spectroscopy (EDS) results (not shown) from the TEM data confirm the presence of gold and ruthenium in the films. High resolution TEM shows that the gold particles are crystalline, and sometimes twinned. The micrograph in Figure 2(b) displays a 6 nm nanocrystal, with the 2.35 Å {111} planes and 1.44 Å {220} planes of face-centred cubic gold clearly visible. The nanocomposite was also characterised with scanning electron microscopy (SEM), which confirmed that the AuNPs had resisted aggregation upon introduction of the RuPc complex (Figure S1).

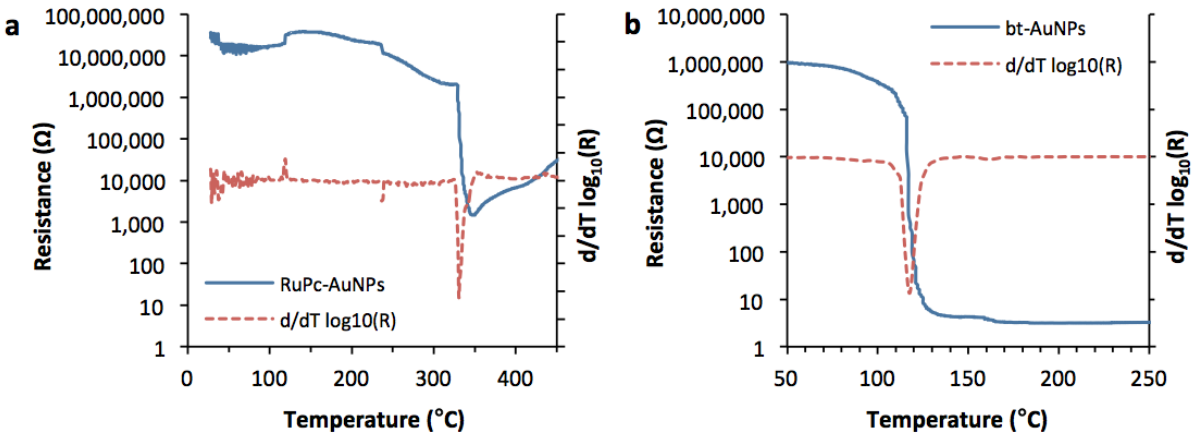

Figure 3. Graphs showing resistance as a function of temperature (solid line) and the calculated derivative (dashed line) for films of (a) RuPc-AuNPs and (b) 1-butanethiol-stabilised AuNPs on thermal oxide coated silicon substrates, heated at 10 °C min^{-1} in air.

Figure 3 shows the resistance of a RuPc-AuNP film as a function of temperature together with data for 1-butanethiol-stabilised gold nanoparticles of a similar diameter for comparison. The sintering event is characterized by a significant drop in resistance. We define the temperature of the sintering event (T_{SE}) as the temperature of maximum rate of change in resistance. In this context, it is important to consider that the sintering of AuNPs is a thermally activated kinetic process and therefore the temperature at which sintering occurs depends on the rate of heating [5]. In the current work, the heating rate was 10 °C min^{-1} for all experiments.

Table 1. Temperature of the sintering event (T_{SE}) for alkanethiol-stabilised AuNPs on glass substrates, heated at 5 °C min^{-1} in air [5].

Alkanethiol	T_{SE} of AuNPs (°C)
2-propanethiol	130
1-butanethiol	150
1-hexanethiol	165
1-nonanethiol	185

The T_{SE} for the RuPc-AuNPs is 320-330 °C (Figure 3(a)), which is ~200 °C higher than that of the 1-butanethiol-stabilised AuNPs (T_{SE} ~120 °C; Figure 3(b)). The T_{SE} of the nanocomposite is also much higher than those of AuNPs stabilised with longer chain alkanethiols, as reported by Coutts, *et al.* (Table 1). The differences in substrate material (glass vs. silicon) and heating rates both act to raise the T_{SE} of the previously reported materials compared to our measurements [5]. We attribute the remarkable increase in T_{SE} of the new nanocomposite, compared to conventional alkanethiol-stabilised particles, to the stability of the RuPc stabilising ligands, which is discussed in detail below. The resistance of the RuPc-AuNP films before sintering is also significantly higher than that of films formed from 1-butanethiol-stabilised NPs. This is attributed to a greater separation of particles in the former case due to the larger size and greater abundance of the stabilising RuPc molecules compared to the 1-butanethiol stabiliser [5]. The resistance of the RuPc-AuNP films after sintering and up to 450 °C (near the limit of our heating apparatus) is also higher than that of films formed from 1-butanethiol-stabilised NPs (~1.5 kΩ vs. ~3 Ω). We attribute this to residual ruthenium oxide compounds that remain at temperatures above the T_{SE}. RuPc-AuNPs continue to lose mass when heated at temperatures up to 1300 °C (see below) and so material from the RuPc decomposition remains in the film even at temperatures 100 °C beyond T_{SE}. Residual material can also be seen in SEM images of the sintered RuPc-AuNP films (Figure S2). In contrast, most of the residue from 1-butanethiol-stabilised particles is volatilised when heated to 250 °C in air, leading to more conductive gold films [6].

EDS during SEM experiments was performed using a sample of RuPc-AuNPs before and after sintering (Figures S3 and S4). Before sintering, sulfur and ruthenium were present in a roughly 1:1 atomic ratio, as expected from the stoichiometry of the RuPc complex, along with a high concentration of carbon and nitrogen (Tables S1 and S2). After sintering, the amounts of sulfur, carbon and nitrogen decreased dramatically, while ruthenium remained in

the same ratio to gold as it had been prior to sintering (Tables S3 and S4), which supports our interpretation of the thermogravimetric analysis (TGA) data.

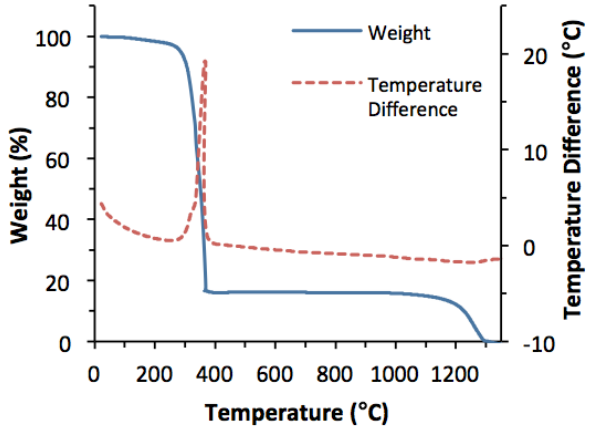

Figure 4. TGA/DSC data for [RuPc(4-py$(CH_2)_3$SAc)(4-py^{t}Bu)], heated at 10 °C min^{-1} in air.

Simultaneous TGA and differential scanning calorimetry (DSC) was utilised to examine the changes occurring to the films upon heating. First, an examination of the TGA/DSC data for [RuPc(4-py$(CH_2)_3$SAc)(4-py^{t}Bu)] (Figure 4) is illustrative. Up to ~330 °C, a mass loss of ~35% was recorded with a relatively small exothermic event at 337 °C. This mass loss corresponds to the removal of the two axial pyridyl ligands, a process that has been utilised by synthetic chemists to prepare four-coordinate RuPc [17]. By 400 °C, a total of 85% of the original mass has been lost with a larger exothermic peak observed at 365 °C. This mass loss is assigned to the combustion of the remaining organic component of the complex, the Pc macrocycle. The remaining mass, ~15%, corresponds to the mass of RuO_2, with the oxygen atoms scavenged from the TGA atmosphere of air. Furthermore, the TGA data between 500 and 1300 °C are quite similar to the reported data for RuO_2 at these temperatures, with a gradual mass loss around 1200 °C [22,23]. At 1300 °C, less than 2% mass remains.

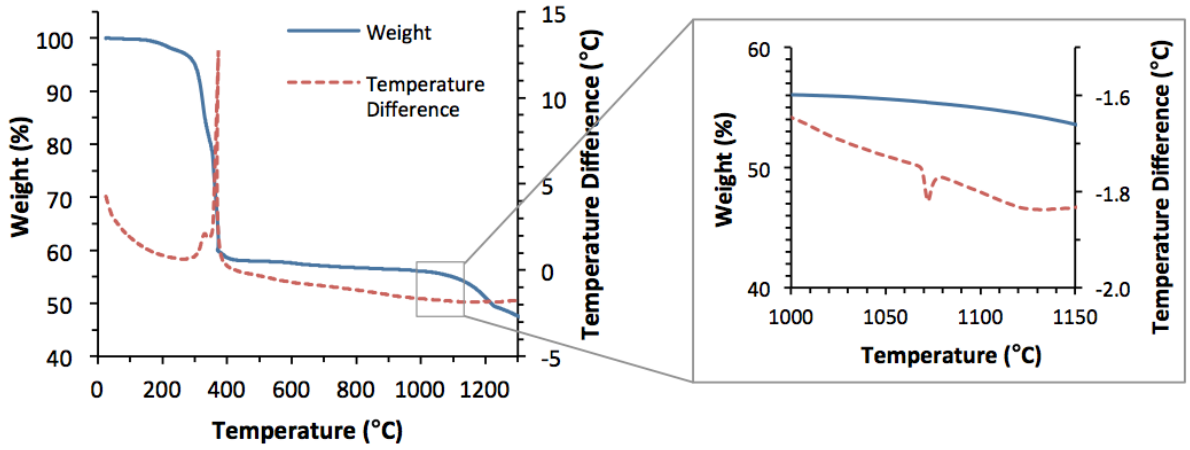

Figure 5. TGA/DSC data for RuPc-AuNPs, heated at 10 °C min^{-1} in air, and the endotherm corresponding to the melting point of gold (inset).

Figure 5 shows simultaneous TGA/DSC data for RuPc-AuNPs. The data display a similar trend to that of the unbound RuPc complex (Figure 5), with exothermic peaks observed at 330 and 373 °C. The total mass loss up to 1300 °C is 53%. The small endothermic feature in the temperature difference data at ~1070 °C corresponds to the melting point of gold (1064 °C). From the data shown in Figures 4 and 5, we conclude that the thermal stability of the RuPc molecules is responsible for the high stability of the RuPc-AuNPs.

The TGA data may also be used to determine the ratio of RuPc molecules per AuNP. A 5 nm diameter AuNP has a calculated mass of 1.26 x 10^{-18} g, while [RuPc(4-py$(CH_2)_3$SAc)(4-py^{t}Bu)] has a mass of 1.57 x 10^{-21} g $molecule^{-1}$. The 53% mass loss (assigned to the RuPc complex) measured by TGA therefore corresponds to 1.42 x 10^{-18} g of RuPc complex per AuNP, or an average of ~900 RuPc molecules per nanoparticle. This number is significantly greater than the number of RuPc molecules that could form a surface-bound monolayer based on geometric considerations (~70, based on an area of ~2.25 nm^2 $molecule^{-1}$ with no overlap of Pc rings) and is not unexpected given the propensity of Pc molecules to form aggregates [24]. Importantly though, this indicates that prior to heating, the gold nanoparticles are well separated by an effective barrier of thermally-stable molecules.

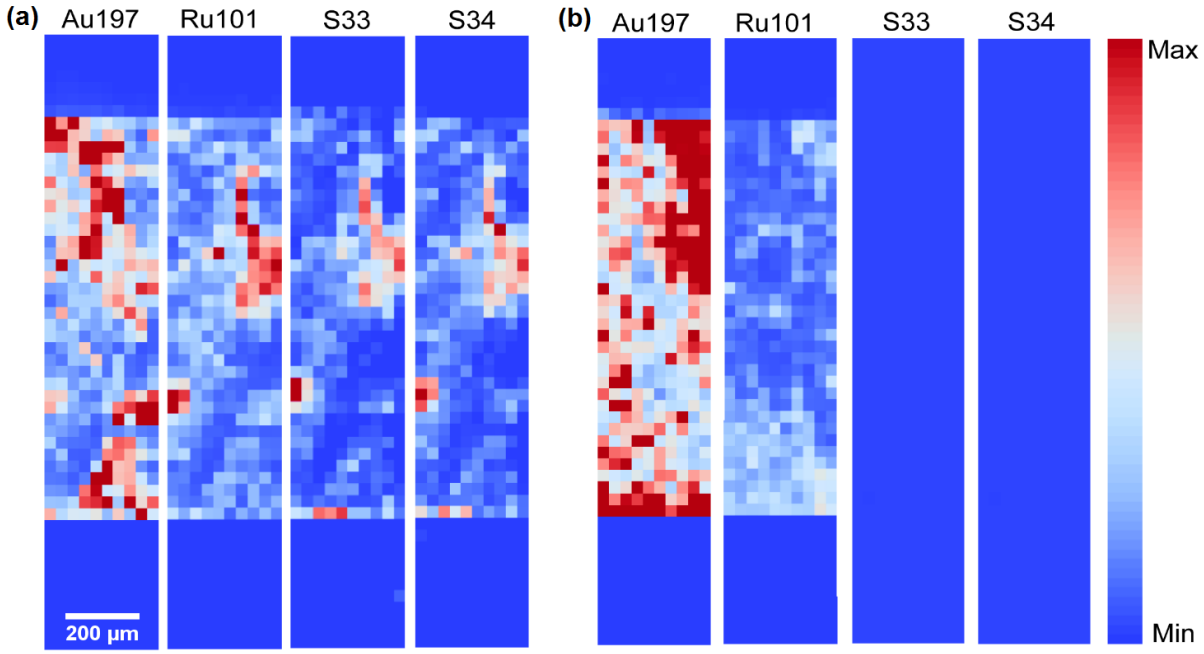

Figure 6. LA-ICP-MS maps of (a) pre-sintered and (b) post-sintered RuPc-AuNPs, with the intensities normalised to Au197.

Laser ablation inductively coupled plasma mass spectrometry (LA-ICP-MS) was used to map the elements of interest on RuPc-AuNP surfaces pre- and post-sintering. The pre-sintered elemental maps show colocalisation of the elements gold, ruthenium, and sulfur (Figure 6(a)). The post-sintered elemental maps contain no detectable sulfur (Figure 6(b)). Gold and ruthenium were still present after sintering, consistent with the EDS data. A larger section of post-sintered RuPc-AuNPs was ablated (Figure S5) and confirmed the observation that levels of sulfur were below the limits of detection in the sintered substrate.

Conclusion

We have shown that gold nanoparticles can be stabilised against sintering to surprisingly high temperatures using suitable protective ligands. In this case, a ruthenium phthalocyanine complex acts as a robust physical barrier to the sintering process where sintering only occurs close to the decomposition temperature of the stabilising molecules.

Experimental Section

General: Potassium thioacetate (Sigma Aldrich), potassium carbonate (Chem-Supply), 4-*tert*-butylpyridine (Sigma Aldrich), dichloromethane (Chem-Supply), toluene (Chem-Supply) and dimethylformamide (Sigma Aldrich) were used as received. Gold(III) chloride [25], oleylamine-stabilised gold nanoparticles [26], bis(benzonitrile)ruthenium phthalocyanine [27] and 4-bromopropylpyridine hydrobromide [28] were prepared by literature procedures. UV-visible spectra were recorded using an Agilent Technologies Cary 100 UV-visible spectrophotometer with toluene as the solvent. Simultaneous thermogravimetric analysis and differential scanning calorimetry was performed using a TA Instruments SDT Q600. Samples weighing 3 – 6 mg were loaded into alumina crucibles and heated from 30 to 1300 °C at 10 °C min^{-1} in air at a flow rate of 25 mL min^{-1}. The transmission electron microscopy study of gold nanoparticles drop cast from toluene onto lacey carbon grids was performed with a JEOL 2200FS TEM operating at 200 kV. Scanning electron microscopy was performed using a Zeiss Supra 55VP SEM operating at 20 kV, with samples drop cast onto silicon wafer. Energy dispersive spectroscopy was performed using a Zeiss Evo LS15 SEM equipped with a Bruker SDD XFlash 5030 detector, using an accelerating voltage of 8 kV, and semi-quantitative analysis results were obtained by using the ZAF correction technique. Laser ablation inductively coupled plasma mass spectrometry was performed using a New Wave UP213 laser ablation unit (Kenelec Technologies) connected to an Agilent Technologies 7500ce ICP-MS. The UP213 unit used an Nd:YAG emission source emitting a nanosecond laser pulse in the fifth harmonic at 213 nm. A standard New Wave ablation cell was used. The carrier gas was argon, flowing through the chamber at 1.15 L min^{-1}. The 7500ce ICP-MS was fitted with a 'cs' lens system for enhanced sensitivity. Forward RF power was reduced to 1250 W for dry plasma conditions. Operational parameters for the LA-ICP-MS system are summarised in Table S5. The following elements were measured: ^{197}Au, ^{101}Ru, ^{33}S and ^{34}S.

Synthesis of *S*-[3-(pyridin-4-yl)propyl]ethanethioate (4-py(CH_2)$_3$SAc): Potassium thioacetate (350 mg, 3.05 mmol), 4-bromopropylpyridine hydrobromide (736 mg, 2.60 mmol) and potassium carbonate (690 mg, 5.02 mmol) were stirred under a nitrogen atmosphere in a 25ml round bottom flask containing 15 ml of dimethylformamide for 18 hours in the dark. The resultant mixture was transferred into a 50 ml separating funnel and toluene (15 mL) was added and the funnel was shaken, followed by the addition of water (15 ml). The mixture was shaken again and the aqueous layer was discarded. The organic layer was washed an additional three times with water (15 mL). The organic layer was dried with magnesium sulphate and then filtered. The solvent was removed using a rotary evaporator at 60^{o}C yielding a light brown oil (68%) which was sufficiently pure to use in the next step. MS (m/z) 197.0803([M+H]$^+$, 21%). ^{1}HNMR (δ 500MHz, $CDCl_3$) 1.92 (p, J_{HH} = 7.5Hz, 2H, CH_2-CH_2), 2.35 (s,3H, CH_3CO); 2.69(t, J=7.5Hz, CH_2Py); 2.89(t, J=7.5Hz, 2H, CH_2Br); 7.12(d, J=5Hz, 2H, PY); 8.5 (d, J=4.5Hz, 2H, PY). IR ν(cm^{-1}) 3023, 2925, 2855, 1690, 1601, 1414, 1134, 952, 667,624. UV-vis (λ_{max} (nm) [ε (L mol^{-1} cm^{-1})]); 230 [13170], 255 [6423].

Synthesis of [RuPc(4-py(CH_2)$_3$SAc)(4-py^{t}Bu)]: Dichloromethane (40ml) was placed in a 250ml 2-neck round bottom flask and deoxygenated by sparging with nitrogen gas. *S*-[3-(pyridin-4-yl)propyl] ethanethioate (76 mg, 0.39 mmol) was added followed by 4-tert-butylpyridine (60 μL, 0.39 mmol) and bis(benzonitrile)ruthenium phthalocyanine (165 mg, 0.270 mmol). The resultant solution was heated at reflux for 3hr under a nitrogen atmosphere the solvent was then removed in vacuo. The crude product was purified by silica column chromatography eluting with dichloromethane : hexane (3:1). The second band to elute was collected and the solvent removed to afford 40 mg (26 %) of blue powder. MS (m/z) 945.2382([M+H] $^+$, 100%). ^{1}HNMR (δ 500MHz $CDCl_3$); 0.31 (s, 9H, t-Bu), 0.88 (P, J=6.5 Hz, 2H, CH_2-CH_2-CH_2); 1.47 (t, J= 7.0Hz, 4H, CH_2-Ph); 2.05 (s, 3H, CH_3CO); 2.17 (t, J=6.5Hz,2H, CH_2S); 2.37 (d, JHH = 6.0 Hz, 4H, py); 5.04 (d, JHH = 6.5 Hz, 2H, py); 5.18 (d, JHH= 7.2 Hz, 2H,

py); 7.88 (m, 8H, Pc); 9.13 (m, 8H, Pc). IR ν(cm^{-1}) 3434, 3052, 2923, 1689, 1652, 1615, 1578, 1489, 1473, 1414, 1366, 1324, 1288, 1168, 1125, 1065, 778, 754, 736, 667, 625, 573. UV-vis (λ_{max} (nm) [ε (L mol^{-1} cm^{-1})]); 316 [112000], 377 [31900], 570 [29900], 625 [80600].

Synthesis of AuNPs functionalised with [RuPc(4-py(CH_2)$_3$SAc)(4-py^{t}Bu)]: [RuPc(4-py(CH_2)$_3$SAc)(4-py^{t}Bu)] (5.2 mg) was added to a suspension of oleylamine-stabilised gold nanoparticles (10.4 mg) in toluene (30 mL) and stirred overnight at room temperature under a nitrogen atmosphere. The functionalised AuNPs were precipitated by the addition of ethanol (90 mL) and collected by centrifugation. The particles were washed three times with ethanol to remove the displaced oleylamine, and then dried under a gentle stream of nitrogen to give a black powder (12 mg).

Electrical resistance measurements: Gold electrodes were formed on thermal oxide-coated silicon substrates (1 cm x 2 cm rectangles) using a length of copper wire (0.5 mm diameter) as a mask and thermally evaporating gold onto the surface (thickness 50 – 100 nm, evaporator base pressure = 2 x 10^{-6} Torr). The edges of the silicon substrates were masked with tape to avoid short circuits across the conductive underside of the substrate. The resultant structures comprised two electrodes separated by a gap of ~0.5 mm spanned by drop-cast films (~5 – 10 mm in diameter).

RuPc-AuNPs were dispersed in the minimum amount of chloroform (concentration ~0.3 g/L) and then deposited using a fine-tipped pipette such that the film spanned the two gold electrodes and a continuous layer of AuNPs remained once the solvent evaporated. The samples were placed on an aluminium heating block with an attached thermocouple. Steel probes (held in place by electromagnet clamps) provided ohmic electrical contact to each of the gold electrodes and resistance was measured using a Yokogawa 7562 digital multimeter

(max. reading 200 MΩ). A LabVIEW program was used to control the heating rate and record temperature and electrical resistance. The temperature was increased at a rate of 10 °C min^{-1} from room temperature to ~100 °C higher than the observed sintering event, which is characterised by a sharp drop in resistance and a colour change of the sample from dark blue to lustrous gold. Each experiment was performed in duplicate to ensure the results were reproducible.

LA-ICP-MS preparation and imaging procedure: A laser beam diameter of 30 µm was used for all experiments, with a scan speed of 30 µm/s and frequency of 20 Hz. The distance between each line was 30 µm to ensure total ablation of the sample sections. An area of 1 mm by 300 µm was ablated on RuPc-AuNP and uncoated control substrates before and after sintering. Finally, a 1.5 mm by 3.4 mm section of post-sintered RuPc-AuNPs was ablated (Table S5).

Each line of ablation generated a single data file for all selected elements. Interactive Spectral Imaging Data Analysis Software (ISIDAS), an in-house developed suite written in the Python programming language was used to amalgamate all data files into a single image. Images were exported from ISIDAS in a Visualization Toolkit (.vtk) format to ParaView 4.3.1 (Kitware Inc.). Relative intensity was determined using Paraview to normalise all elemental maps to the Au197 map.

Acknowledgements

We acknowledge Roc Matthieu, Ropeta Hunt, Jean-Pierre Guerbois, Dr David Bishop, Geoff McCredie, and Katie McBean for their assistance. The authors acknowledge the facilities and the scientific and technical assistance of the Australian Microscopy & Microanalysis Research Facility at the Australian Centre for Microscopy & Microanalysis at the University of Sydney.

References

1. Saha, K.; Agasti, S. S.; Kim, C.; Li, X.; Rotello, V. M. Gold nanoparticles in chemical and biological sensing. *Chem. Rev.* **2012**, *112*, 2739–2779.

2. Ko, H.; Singamaneni, S.; Tsukruk, V. V. Nanostructured surfaces and assemblies as SERS media. *Small* **2008**, *4*, 1576–1599.

3. Daniel, M.-C.; Astruc, D. Gold nanoparticles: assembly, supramolecular chemistry, quantum-size-related properties, and applications toward biology, catalysis, and nanotechnology. *Chem. Rev.* **2004**, *104*, 293–346.

4. Zhang, J. Z.; Noguez, C. Plasmonic optical properties and applications of metal nanostructures. *Plasmonics* **2008**, *3*, 127–150.

5. Coutts, M. J.; Cortie, M. B.; Ford, M. J.; McDonagh, A. M. Rapid and controllable sintering of gold nanoparticle inks at room temperature using a chemical agent. *J. Phys. Chem. C* **2009**, *113*, 1325–1328.

6. Cortie, M. B.; Coutts, M. J.; Ton-That, C.; Dowd, A.; Keast, V. J.; McDonagh, A. M. On the coalescence of nanoparticulate gold sinter ink. *J. Phys. Chem. C* **2013**, *117*, 11377–11384.

7. Smith, B. L.; Hutchison, J. E. Transformations during sintering of small (D_{core} < 2 nm) ligand-stabilized gold nanoparticles: influence of ligand functionality and core size. *J. Phys. Chem. C* **2013**, *117*, 25127–25137.

8. Liana, D. D.; Raguse, B.; Wieczorek, L.; Baxter, G. R.; Chuah, K.; Gooding, J. J.; Chow, E. Sintered gold nanoparticles as an electrode material for paper-based electrochemical sensors. *RSC Adv.* **2013**, *3*, 8683–8691.

9. Deng, M.; Zhang, X.; Zhang, Z.; Xin, Z.; Song, Y. A gold nanoparticle ink suitable for the fabrication of electrochemical electrode by inkjet printing. *J. Nanosci. Nanotechnol.* **2014**, *14*, 5114–5119.

10. Polavarapu, L.; Manga, K. K.; Yu, K.; Ang, P. K.; Cao, H. D.; Balapanuru, J.; Loh, K. P.; Xu, Q.-H. Alkylamine capped metal nanoparticle “inks” for printable SERS substrates, electronics and broadband photodetectors. *Nanoscale* **2011**, *3*, 2268–2274.

11. Puértolas, B.; Mayoral, Á.; Arenal, R.; Solsona, B.; Moragues, A.; Murcia-Mascaros, S.; Amorós, P.; Hungría, A. B.; Taylor, S. H.; García, T. High-temperature stable gold nanoparticle catalysts for application under severe conditions: the role of TiO_2 nanodomains in structure and activity. *ACS Catal.* **2015**, *5*, 1078–1086.

12. Lee, I.; Joo, J. B.; Yin, Y.; Zaera, F. A yolk@shell nanoarchitecture for Au/TiO_2 catalysts. *Angew. Chem.* **2011**, *123*, 10390–10393.

13. Joo, S. H.; Park, J. Y.; Tsung, C.-K.; Yamada, Y.; Yang, P.; Somorjai, G. A. Thermally stable Pt/mesoporous silica core-shell nanocatalysts for high-temperature reactions. *Nat. Mater.* **2009**, *8*, 126–31.

14. Dick, K.; Dhanasekaran, T.; Zhang, Z.; Meisel, D. Size-dependent melting of silica-encapsulated gold nanoparticles. *J. Am. Chem. Soc.* **2002**, *124*, 2312–2317.

15. De la Torre, G.; Claessens, C. G.; Torres, T. Phthalocyanines: old dyes, new materials. Putting color in nanotechnology. *Chem. Commun.* **2007**, 2000–2015.

16. Nyokong, T.; Antunes, E. Influence of nanoparticle materials on the photophysical behavior of phthalocyanines. *Coordin. Chem. Rev.* **2013**, *257*, 2401–2418.

17. Rawling, T.; McDonagh, A. Ruthenium phthalocyanine and naphthalocyanine complexes: synthesis, properties and applications. *Coordin. Chem. Rev.* **2007**, *251*, 1128–1157.

18. Han, M.; Zhang, X.; Zhang, X.; Liao, C.; Zhu, B.; Li, Q. Azo-coupled zinc phthalocyanines: towards broad absorption and application in dye-sensitized solar cells. *Polyhedron* **2015**, *85*, 864–873.

19. Rawling, T.; Austin, C. E.; Hare, D.; Doble, P. A.; Zareie, H. M.; McDonagh, A. M. Thin films of ruthenium phthalocyanine complexes. *Nano Res.* **2009**, *2*, 678–687.

20. Turkevich, J. Colloidal gold. Part II colour, coagulation, adhesion, alloying and catalytic properties. *Gold Bull.* **1985**, *18*, 125–131.

21. Stuzhin, P. A.; Vagin, S. I.; Hanack, M. Synthesis and Spectral Properties of Bisaxially Coordinated (Octaphenyltetraazaporphyrinato)ruthenium(II) Complexes. *Inorg. Chem.* **1998**, *37*, 2655–2662.

22. Rolison, D. R.; Hagans, P. L.; Swider, K. E.; Long, J. W. Role of hydrous ruthenium oxide in Pt - Ru direct methanol fuel cell anode electrocatalysts: the importance of mixed electron/proton conductivity. *Langmuir* **1999**, *15*, 774–779.

23. Campbell, P. F.; Ortner, M. H.; Anderson, C. J. Differential thermal analysis and thermogravimetric analysis of fission product oxides and nitrates to 1500 °C. *Anal. Chem.* **1961**, *33*, 58–61.

24. Snow, A. W. Phthalocyanine Aggregation. In *The Porphyrin Handbook. Phthalocyanines: Properties and Materials*; Kadish, K. M.; Smith, K. M.; Guilard, R., Eds.; Academic Press: New York, 2003; p. 130.

25. King, S. R.; Massicot, J.; McDonagh, A. M. A straightforward route to tetrachloroauric acid from gold metal and molecular chlorine for nanoparticle synthesis. *Metals* **2015**, *5*, 1454–1461.

26. Choi, H.; Chen, W. T.; Kamat, P. V Know thy nano neighbor. Plasmonic versus electron charging effects of metal nanoparticles in dye-sensitized solar cells. *ACS Nano* **2012**, *6*, 4418–4427.

27. Bossard, G. E.; Abrams, M. J.; Darkes, M. C.; Vollano, J. F.; Brooks, R. C. Convenient synthesis of water soluble, isomerically pure ruthenium phthalocyanine complexes. *Inorg. Chem.* **1995**, *34*, 1524–1527.

28. Elpern, B.; Gardner, L. N.; Grumbach, L. Strong analgesics. The preparation of some ethyl 1-aralkyl-4-phenylpiperidine-4-carboxylates. *J. Am. Chem. Soc.* **1957**, *79*, 1951–1954.